Superdrawing of Ultrahigh Molecular Weight Polyethylene. 1. Effect of Techniques on Drawing of Single Crystal Mats

Tetsuo Kanamoto, Akeharu Tsuruta,† Koji Tanaka, and Masatami Takeda

Department of Applied Chemistry, Science University of Tokyo, Kagurazaka, Shinjuku-ku, Tokyo 162, Japan

Roger S. Porter*

Polymer Science and Engineering Department, University of Massachusetts, Amherst, Massachusetts 01003. *Received February 2, 1987; Revised Manuscript Received July 20, 1987*

ABSTRACT: Single crystal mats of ultrahigh molecular weight polyethylene (UHMW-PE) have been uniaxially drawn by three techniques: solid-state coextrusion, tensile drawing, and the combination of the two. The drawability and the resultant structure and properties of superdrawn films were found to be sensitive to drawing technique. Tensile drawing was markedly influenced by the coherency of the mats and the draw temperature and rate. Draw ratios (DR) over 200 at ≥90 °C under controlled rates have been achieved for coherent mats. Effective draw was not possible for less coherent mats and for all drawn at ≤60 °C. These conventionally drawn films had a single crystal-like texture; those prepared by solid-state extrusion or by two-stage draw showed uniaxial orientation. The mats could be effectively drawn even at 50 °C up to a DR of 35. The most efficient and highest draw has been achieved by first solid-state coextrusion of mats to a low DR of 6, followed by tensile drawing at elevated temperatures. The tensile modulus and strength of such two-stage drawn films increase rapidly with DR in the lower DR range of <150 and approach a constant value of 210–220 and 4.0 GPa, respectively, at higher a DR of ≥200–250. With a density of one, these polyethylenes have among the highest and perhaps the highest known specific moduli and strengths, respectively. Such superdrawn, ultrahigh modulus films of UHMW-PE exhibit extremes of chain extension and orientation. The morphological perfection has been assessed by wide- and small-angle X-ray diffraction, density, DSC heat of fusion, etc. The similarities and differences in the structure and drawing of single crystal mats versus gels of UHMW-PE are also discussed.

Introduction

During the past decade, remarkable progress has been made in the development of high modulus and strength morphologies by uniaxial drawing of flexible chain polymers.[1-4] Several techniques for ultradrawing of semicrystalline polymers have been developed, including solid-state extrusion[5-7] and tensile drawing.[8,9] Techniques have generally been applied to the drawing of melt-crystallized forms of normal molecular weight (MW) polymers. The most extensively studied has been high density polyethylene (HDPE). Here it has been established that the tensile properties of effectively drawn HDPF increase steadily with draw ratio (DR).[5-9] The maximum achievable DR for melt-crystallized morphologies of higher MW HDPE has been limited by a decreasing ductility with increasing MW. The tensile strength at a given DR is enhanced, nonetheless, on increasing sample MW.[10] There is thus a continuing effort to achieve the highest possible mechanical properties and hence the highest possible DR.

Pennings et al.[1,11] have produced ultrahigh modulus and strength polyethylene fibers by flow-indicated crystallization from solutions and post-drawing of ultrahigh MW polyethylene (UHMW-PE). Smith et al.[12,13] have shown that UHMW-PE gels prepared by quenching semidilute solutions can be highly drawn, up to a DR of 130, depending on the initial polymer concentration. These highly drawn films exhibited tensile moduli and strength up to 150 and 3 GPa, respectively.[13] Even the highest modulus achieved, however, is still well below the broad range of theoretical moduli reported for a perfect polyethylene crystal, 220–324 GPa.[14-16]

Porter with his collaborators[1,2,6,17] have extensively studied the effect of extrusion variables including initial morphology on solid-state extrusion of HDPE. In an extension of these studies, Kanamoto et al.[18] found that single crystal mats and powders, grown from dilute solutions, could be extrusion drawn up to a DR over that for melt-crystallized spherulitic morphologies (DR 45 versus 30 at 110 °C). The DR achieved by the solid-state extrusion was significantly higher than that reported by the tensile draw of HDPE morphologies, including single crystal mats.[19,20] On the basis of this, we have examined the drawability of UHMW-PE single crystal mats,[21,22] grown from dilute solutions. It was found that mats could be drawn up to a DR 250, by utilizing two-stage drawing, i.e., solid-state coextrusion[23] followed by tensile drawing at controlled temperatures and rates. Such superdrawn films exhibit ambient tensile moduli of ≤222 GPa,[21] approaching the lowest reported theoretical modulus for polyethylene crystals.[14-16] Subsequently, Miyasaka et al.[25] and Matsuo et al.[16,26] reported similarly high DR and moduli on drawing UHMW-PE single crystal mats and gels, respectively, both prepared from dilute solutions. A continuing study for the improvement of drawing conditions has resulted in superdrawn films of UHMW-PE, of DR 350 and over, with the corresponding tensile moduli and strength up to 220 and 6.5 GPa, respectively, for the highest molecular weight.[27] It has been also shown that superdrawn films of UHMW-polypropylene, exhibiting tensile moduli (≤33 GPa) and approaching the crystal lattice modulus (34–42 GPa[14]), could be prepared by drawing solution-grown crystal (SGC) mats.[24] The objective of this paper is to report the significant effects of drawing technique on the uniaxial drawing of UHMW-PE SGC mats and discuss the resultant tensile properties and limiting morphology of superdrawn films. The remarkable effect of polyethylene MW on the drawing behavior and tensile properties and on changes in morphology and physical properties are to be reported in companion papers.

Experimental Section

Samples. The UHMW-PE used was Mitsui Hizex Million 240 M having a viscosity average molecular weight (M_v) of 1.6×10^6, unless otherwise noted. In a few experiments, Hercules Hifax

† Present address: Polymer Research Laboratory, Toyo Soda Industry Company, Kasumi, Yokkaichi, Mie 510, Japan.

0024-9297/88/2221-0470$01.50/0

1900 with an M_v of 2.1×10^6 was used. Solution-grown crystals (SGC) of UHMW-PE were isothermally precipitated from dilute solutions (0.05 and 0.2 wt %) in xylene kept at 85 °C. Several precautions were taken for solution crystallization. The polymer solutions were stabilized with 0.1 wt % (based on the solvent) of an antioxidant, 2,6-di-*tert*-butyl-*p*-cresol. A mixture of the requisite amount of UHMW-PE and antioxidant plus 350 mL of xylene in a 500-mL conical flask was heated with slow stirring under an N_2 gas flow, up to the boiling point and held there for 15 min. The solution was then quenched in tap water to assess the complete dissolution of the polymer. The gel-like suspension, thus obtained, was again heated, without stirring, under an N_2 gas flow and kept at 135 °C for 15 min to obtain a homogeneous solution. The flask containing the hot solution was transferred to a silicone oil bath at 85 °C and kept over 20 h to consolidate crystallization. Sedimented mats of SGC were obtained by slowly filtering the crystal suspension at room temperature followed by drying in vacuo at 50 °C.

Drawing. Three techniques have been utilized for drawing SGC mats: i.e., solid-state coextrusion,[23] conventional tensile drawing, and two-stage drawing (their sequential combination). For solid-state coextrusion, one or more mats ($9 \times 0.3 \times 70$ mm) were placed between two longitudinally split billet halves of HDPE and the assembly coextruded at constant temperatures of 20–135 °C through conical brass dies having nominal extrusion draw ratios (EDR) of 3–25. Coextrusion was conducted at constant pressures of 20–230 MPa. The drawability of the mats were limited by the lower deformability of the substrate HDPE. Coextrusion was thus repeated two or three times to achieve the desired EDR. The total EDR after coextrusion was determined from the separation of ink marks preimprinted on the surface of a mat or extrudate.

For straight tensile drawing, a mat with 2 mm wide and 0.3 mm thick was drawn in an air oven equipped with a Tensilon tensile tester UTM-100 at constant extension cross-head speeds (CHS) of 1–100 mm/min and at constant temperatures over 60–130 °C. For two-stage drawing, SGC mats were first drawn by solid-state coextrusion up to an EDR of 6–25 at 110 °C, and these extrudates were further drawn at a constant CHS and at 20–130 °C. The total draw ratio (DR_t) was defined by EDR × DR.

Measurements. The tensile modulus and strength on the fiber axis for drawn films were measured at room temperature and at strain rates of 1×10^{-3} and 1×10^{-2} s^{-1}, respectively. The modulus was determined from the tangent to the stress–strain curve at a low strain (≤0.1%). The cross-sectional area of a sample (10^{-1}–10^{-3} mm^2) was calculated from the sample weight, length, and measured density. Density was measured at 30 °C in a density gradient column consisting of the mixtures of methylcarbitol and butylcellosolve.

Wide- (WAXD) and small-angle X-ray scattering (SAXS) patterns were recorded on a flat plate camera and a JEOL small-angle vacuum camera, respectively. Ni-filtered Cu Kα radiation was used.

The molecular weight and distribution, before and after superdrawing of SGC mats, were measured with a Waters Associates, Inc, GPC Model 150C at 140 °C using *o*-dichlorobenzene solvent containing 0.1% of antioxidant. Molecular weight calibration was made with narrow distribution polystyrene standards. The GPC flow rate was ~0.5 mL/min. The polymer concentration was 0.02%.

Results and Discussion

Drawing of SGC Mats and Gels. The SGC mats of UHMW-PE formed from a 0.05 wt % solution in xylene were usually translucent and uniform. However, the mats from more concentrated solution, 0.2 wt %, were less uniform and often opaque, suggesting a poor coherency of crystal lamellae in the mats. Independent of appearance, the WAXD and SAXS patterns showed lamellae of ~140 Å thickness that were well oriented with the fold surface parallel to the mat surface and with the molecular chains perpendicular to the surface. The mat density was 0.971–0.974 g/cm^3, corresponding to a crystallinity of 83–84 wt %. These features of UHMW-PE SGC mats are similar to the well-known single crystal mats of HDPE.[28] However, the mats of UHMW-PE were ductile under some conditions, as opposed to those of HDPE which are usually brittle.

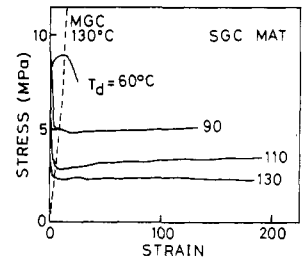

Figure 1. Nominal stress versus strain curves for tensile drawing of UHMW-PE SGC mats at a constant CHS of 1 cm/min and at 60–130 °C. The draw stress for a melt-crystallized (MGC) at 130 °C is also included.

The similarities and differences between single crystal aggregates and gels of UHMW-PE should first be summarized. The gel is usually prepared by quenching semidilute solutions (≥1 wt %) giving a macroscopically coherent structure due to the formation of crystalline junctions and chain entanglements, depending on the concentration of solution from which gel is generated. This coherence of gels is a major difference in the structure from single crystals precipitated from dilute solutions, where each crystal is isolated in the crystal suspension.

Smith et al.[13] reported that the orientation of lamellar crystals in a dried gel depends on the method of solvent removal. When the solvent was extracted from a gel by a low boiling solvent and subsequently dried, a highly porous and opaque material is obtained, in which lamellae are oriented randomly. However, when a gel is dried slowly at ambient conditions, a coherent gel film is obtained, in which lamellae are well oriented as commonly observed in polyethylene SGC mats. Importantly, they found no difference in the tensile drawing behavior between dried gels prepared by either of the two methods. Thus the importance of the chain entanglement density is emphasized, which depends on the initial polymer concentration.[12] Such differences in gel structure cause significant differences in drawing between gels and single crystal aggregates, as discussed below. Although both the SGC mats and the dried gels consist of well-developed lamellar crystals,[12,26] further differences in the structure are likely. The former crystals are slightly thicker (140 versus 110 Å) and thermally more stable and may have a more perfect structure than the latter reflecting their higher temperature and the lower solution concentration for crystallization from solution.

Tensile Drawing of SGC Mats. Tensile drawing of SGC mats is significantly affected by the sample preparation, which includes the coherency of lamellae in the mats. Mats formed from 0.05 wt % solution exhibited a good reproducibility in drawing, whereas those from 0.2 wt % solutions showed poor reproducibility, likely due to the less coherent lamellar packing. Thus tensile drawing was performed only on the mats formed from 0.05 wt % solutions.

Figure 1 shows nominal stress versus strain curves for tensile drawing of UHMW-PE SGC mats recorded at constant temperatures over the 60–130 °C range. Mats of 1-mm gauge length were drawn at a CHS of 10 mm/min. At temperatures ≤60 °C the draw was found to be unstable with no effective draw possible for tensile drawing of the mats. However, at ≥90 °C, mats showed excellent drawability. The draw stress initially increased rapidly, followed by a sharp drop after yielding with a sharp neck formation, and then stayed at an almost constant value,

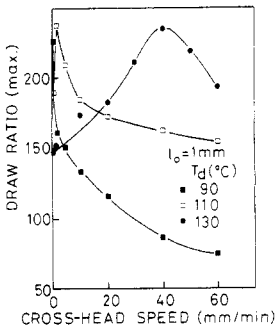

Figure 2. Maximum achievable DR as a function of CHS for tensile drawing of UHMW-PE SGC mats at 90–130 °C. The initial sample length was 1 mm.

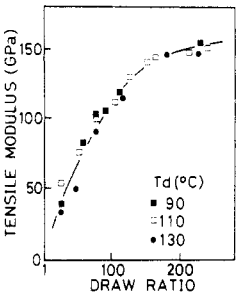

Figure 3. Tensile modulus versus DR for tensile drawing of UHMW-PE SGC mats.

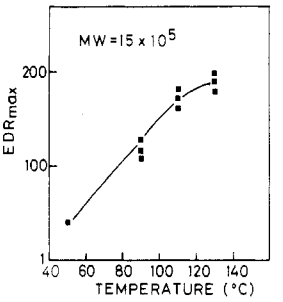

Figure 4. Maximum achievable EDR versus temperature for solid-state coextrusion of UHMW-PE SGC mats.

depending on the drawing temperature and rate. The stress decreased with increasing the drawing temperature or decreasing the drawing rate. The strain hardening phenomenon, usually observed for drawing melt-crystallized polymers, was absent in both the tensile drawing of SGC mats and in the post drawing of the extruded SGC mats, as detailed later. Furthermore, the draw stress was remarkably low, compared to that for draw of a melt-crystallized UHMW-PE. These features are related to the characteristic morphology of solution-grown crystals precipitated from dilute solution. They also explain the dramatic improvement in deformability of UHMW-PE.

The drawability of mats by tensile force was studied as a function of drawing rate at constant temperatures of 90–130 °C, as shown in Figure 2. The maximum achievable DR at 90–110 °C increased steadily with decreasing draw rate. This tendency is greatest at a lower temperature of 90 °C. On lowering draw temperature, the draw stress increases, as shown in Figure 1. Thus, a slower deformation, which produces lower draw stress, allows a higher DR to be achieved (Figure 2). At 130 °C, the drawability with draw rate is complex. The DR increase with increasing draw rate from 150 at a CHS of 1 mm/min to a maximum of 240 at 40 mm/min. It then decreased with increasing test rate. This behavior indicates that two opposing factors may control the drawability of mats. As the draw temperature was increased, chain mobility is increased promoting deformability, and structural reorganization due to annealing becomes significant. It was noted that when a SGC mat was heated up to 130 °C in an air, the mat became transparent and wrinkled due to the partial melting of the thin crystals. The DSC thermogram of the mat also showed an onset of melting below 130 °C. Thus, on heating the mat to draw temperature, a structural reorganization occurs, resulting in a reduction in drawability. This reorganization was most extensive at 135 °C, and it was difficult to draw the mat over a DR off 100. Furthermore, the annealing during deformation is also important, as suggested by the marked effect of draw rates on the maximum attainable DR. This may be partially suppressed by increasing the drawing rate. However, when the rate is increased, the draw stress increases up to the tensile strength of the sample, resulting in fracture. The maximum DR achieved by tensile drawing alone of the coherent mats was ~240.

Figure 3 shows the tensile modulus as a function of DR for tensile drawn mats of UHMW-PE SGC. Irrespective of the draw temperature, 90–130 °C, and rate, the moduli fall on a single curve within experimental error. The modulus increases rapidly with DR at the lower DR range (<150) and then more slowly at higher DR. The maximum modulus achieved by tensile drawing of mats was 160 GPa at DR 240. It has been reported that the modulus at a given DR for HDPE extrudates is higher for extrusion at lower temperatures,[1,6] indicating a higher draw efficiency at lower temperatures. However, the efficiency of draw for UHMW-PE SGC mats was found not to be affected by the temperature as well as the rate, at least below 130 °C. This difference between HDPE and UHMW-PE may be related to the markedly longer relaxation time for the latter which may significantly suppress the relaxation of molecular orientation achieved during deformation.

Solid-State Coextrusion. Figure 4 shows the maximum EDR achieved for UHMW-PE SGC mats by solid-state coextrusion at several temperatures. This EDR increased from 35 at 50 °C to ~200 at 130 °C. The mat initially coextruded to an EDR 6 was followed by successive coextrusions to reach the maximum. For coextrusion at 130 °C, the solution-grown crystals were unstable. The mats were thus initially coextruded at 110 °C, followed by coextrusion at 130 °C. The total EDR achieved did not vary systematically with the EDR used for the second- or third-stage coextrusions.

The pressure of 50–240 MPa applied for extrusion significantly suppressed chain mobility and hence the deformability at a given temperature.[29] This should be considered on comparing drawability by solid-state coextrusion and by tensile drawing (Figures 2 and 4). A remarkable difference in drawing behavior between the two techniques was found at low temperatures. As stated, the tensile drawing of mats at ≤60 °C was unstable. In contrast, solid-state coextrusion allowed effective draw at 50 °C up to an EDR 35, as shown in Figure 4. Furthermore, the mats could be effectively drawn, even at room temperature, up to 27–45 by solid-state coextrusion[30] and by two-stage drawing.[21] These facts indicate that the coherency of crystalline lamellae is an important influence on the drawability, as well as the efficiency of draw, as has also been observed on the solid-state extrusion of HDPE single crystals[18] and on the ultradrawing of UHMW-PE reactor powder.[31] It is thus concluded that the coherent mats exhibit an excellent drawability for both tensile drawing and solid–state coextrusion. However, the efficiency of draw is higher for coextrusion than for tensile

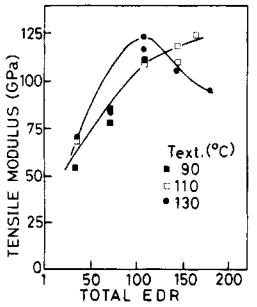

Figure 5. Tensile modulus versus EDR for solid-state coextrusion.

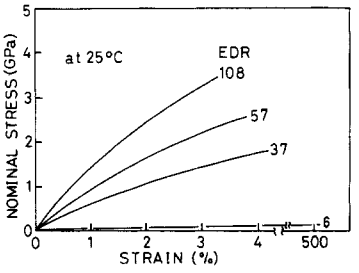

Figure 6. Stress versus strain curves for the ambient tensile testing of solid-state coextruded films. The initial strain rate was 1×10^{-2} s^{-1}. Note the markedly large strain at break for an EDR 6 extrudate.

drawing if the coherency of mats is poor or on draw at lower temperatures.

Figure 5 shows tensile moduli as a function of EDR for solid-state coextrusion of SGC mats performed at 90–130 °C. The modulus increases rapidly with EDR up to 105–120 GPa at an EDR 100. At an EDR ≥ 110, the modulus change is complex; it increases slightly with EDR for extrusion at 110 °C but decreases for extrusion at 130 °C. This could be partly due to the annealing at the high temperature, which depends on the extrusion pressure (and hence the die EDR) and also the time required to achieve the temperature equilibrium (~10 min) before the pressure is applied for extrusion draw. The other factor that may affect the tensile properties is the formation of flaws in superdrawn samples revealed by an optical microscopy. The flaws were not observed at low EDR but appeared most remarkably on superdrawn films, probably due to the complex deformation flow fields.[32]

Two-Stage Drawing. An unusual stress–strain behavior was found during the measurements of the tensile properties of solid-state coextruded SGC mats. Figure 6 shows the stress–strain curves for samples of 6–108 EDR, measured at room temperature. The strain at break increased slightly with decreasing EDR in the EDR range of 108–37. However, it increased abruptly from 4.3% at an EDR 37 to 610% at EDR 6. Thus, SGC mats were initially coextruded to low EDR's of 6, 12, and 25 and subsequently drawn by tensile force at elevated temperatures to examine the effect of initial EDR on the second-stage tensile drawability. As the mats formed from 0.2 wt % solutions also exhibited an excellent drawability like those from 0.05 wt % solutions, the former mats were used for two-stage drawing.

Figures 7 and 8 show the nominal draw stress versus strain recorded at a constant CHS of 10 mm/min and temperatures from 60 to 130 °C for extrudates of an initial EDR 6 and 25, respectively. At constant CHS, the strain rate decreased gradually as the samples were elongated. Thus, the initial sample lengths were adjusted so as to give the same elongation rate for the extrudates having different initial EDR, as each sample passed through any DR_t. Thus, the initial sample lengths were 5, 10, and 20 mm for

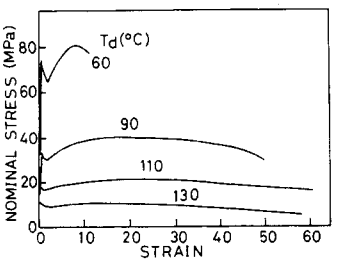

Figure 7. Nominal stress versus strain curves for the second-stage tensile drawing of an EDR 6 extrudate at 60–130 °C.

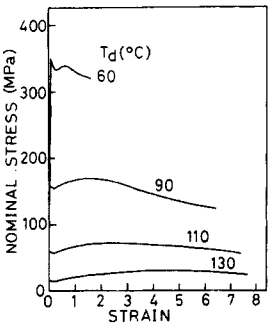

Figure 8. Nominal stress versus strain for the second-stage tensile drawing of an EDR 25 extrudate recorded at 60–130 °C.

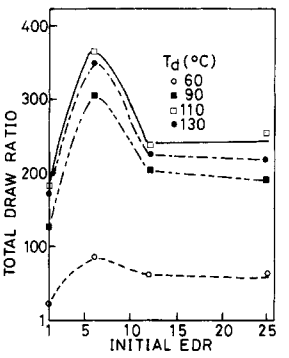

Figure 9. Maximum achievable DR_t as a function of initial EDR for the second-stage tensile drawing of SGC mats observed at a constant CHS of 1 cm/min and at 60–130 °C. The initial sample length for different EDR extrudates was adjusted to give the same extension rate when each sample passed through a given DR_t.

extrudates of EDR 6, 12, and 25 respectively. Each extrudate exhibited a yield point in the stress–strain curves. However, apparently uniform deformation occurred, in contrast to the obvious neck deformation on tensile drawing of SGC mats. After yielding, the nominal draw stress stayed almost constant and showed no strain hardening, as was observed on tensile drawing of mats (Figures 1, 7, and 8).

Figure 9 shows the maximum achieved DR_t initial EDR for draw at temperatures from 60 to 130 °C under conditions described above. The data for EDR = 1 (original SGC mat) were taken from Figure 2, where the mats were formed from 0.05 wt % solutions. Drawability increased markedly between 60 and 90 °C, due to the crystal softening associated with the α-dispersion of SGC mats.[32] At temperatures between 90 and 130 °C, each extrudate exhibited a high drawability, slightly dependent on the combination of drawing temperature and rate. In general, however, extrudate with an initial EDR of 6 was most deformable and over a wide range of drawing temperatures and rates.

Figure 10 shows the effect of extrusion temperature to an EDR of 6 on the maximum DR_t achieved in the second-stage tensile drawing. The SGC mats formed from

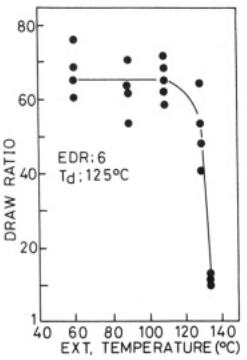

Figure 10. Effect of extrusion temperature on the subsequent tensile drawability at 125 °C for EDR 6 extrudates.

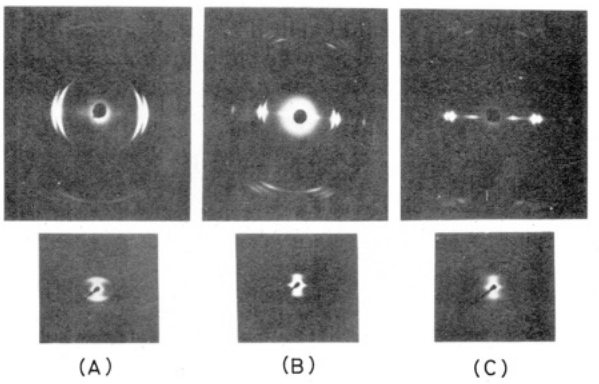

Figure 11. WAXD (top) and SAXS (bottom) patterns of EDR 6 (A), 12 (B), and 25 (C) extrudates.

UHMW-PE with an M_v of 2.1×10^6 was used. The extrudates were 5-mm gauge length were drawn at 125 °C and a constant CHS of 10 mm/min. The averaged maximum DR was ~62 (DR_t of $6 \times 62 = 372$) and not affected by the first-stage extrusion temperatures $\leq$ 110 °C. Further, a $DR_t > 300$ was always achieved even with scatter of data. For extrusion at $\geq$130 °C, the drawability dropped precipitously, likely due to annealing.

The marked improvement in drawability for UHMW-PE SGC mats by solid-state coextrusion at low EDR, 6–25, is ascribed to the enhancement of the coherency of crystalline lamellae or fibrils, as cited above. The reason why an EDR 6 extrudate exhibits a higher drawability over those with EDR $\geq$ 12 is not clear. The true draw stress increased with DR and approached constant values depending on the draw temperatures. This value is calculated by dividing the nominal stress in Figures 7 and 8 by the cross-sectional area of the deforming sample. No systematic effect of initial EDR on the stress was detected within draw temperature variations (~3 °C). Figure 11 shows WAXD and SAXS patterns of EDR 6, 12, and 25 extrudates. The WAXD patterns show that the crystalline chains are well oriented along the fiber axis for EDR $\geq$ 12 yet are remarkably poorer for an EDR of 6. The SAXS patterns also show a less perfect fibrillar structure for an EDR 6 sample compared to the fibrillar morphology for the higher EDR samples (EDR $\geq$ 12). Scanning electron micrographs also revealed morphological features consistent with X-ray diffraction patterns. These facts show that at EDR 6, most of the initial lamellae are inclined and partially broken into smaller crystal blocks of less perfect orientation and fibrillar structure than for fibrils of EDR $\geq$ 12. As discussed by Peterlin,[1,2] macroscopic deformation proceeds through interfibrillar slippage that unravel the successive chain folds of the crystal blocks within microfibrils. It is noted that a higher pressure was applied for extrusion at higher EDR, consistent with higher interfibrillar coherency and adhesion for higher EDR extrudates. Thus, one possible explanation of the effect of initial EDR on the final-stage tensile drawability may be that an intermediate adhesion between fibrils allows an effective and smooth draw which proceeds by the interfibrillar sliding. A more detailed mechanism is not yet clear. However, a similar effect of initial EDR on the second-stage tensile drawability has been observed for drawing SGC mats of other polymers including polypropylene[24] and poly(ethylene terephthalate).[34]

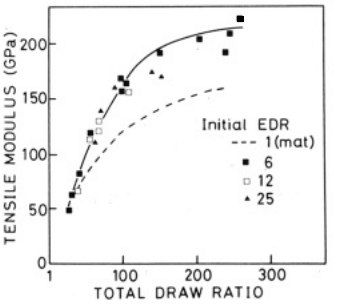

Figure 12. Tensile modulus versus DR_t for doubly drawn films prepared from an initial EDR of 6, 12, and 25. The moduli for tensile drawn mats are also shown by the dotted line.

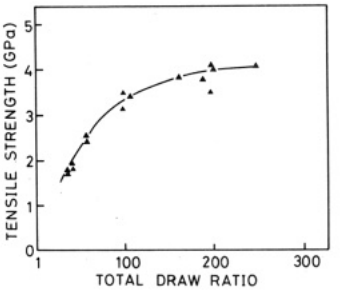

Figure 13. Tensile strength versus DR_t for doubly drawn films.

Figure 12 shows tensile modulus as a function of DR_t for doubly drawn films prepared from an initial EDR of 6, 12, and 25. The data for tensile drawing of the mats are also shown by the dotted line for comparison. Independent of the initial EDR and draw temperatures ($\leq$130 °C), the moduli for two-stage draw fall on a single curve. The modulus increased rapidly with DR_t below a value of 150 and approached a constant of 210–220 GPa at a $DR_t \geq 250$. This maximum is close to the lowest theoretical modulus reported for a perfect polyethylene crystal (220–324 GPa[14-16]). The efficiency of draw, as evaluated by tensile modulus, is remarkably higher for two-stage drawing than for tensile drawing of SGC mats. Miyasaka et al.[25] also have studied tensile drawing of SGC mats of UHMW-PE. Although they compressed the mats before drawing to improve the coherency, they observed a similar relation between dynamic modulus and DR as here. As discussed above, the lower modulus for tensile drawing is likely ascribable to the poorer coherency of the initial lamellae in the mats and also of the resultant fibrils formed by the destruction of the lamellae. The poor coherency may reduce the efficiency of molecular deformation. Figure 13 shows the tensile strength (force at break) as a function of DR_t for the two-stage process. The strength is sensitive to the method of measurement. In the initial report,[21] the superdrawn films always fractured at the edge of the cramp and at a low strain ($\leq$1%), resulting in the apparently lower tensile strength of 0.9–2.0 GPa. In this work, the sample ends were sandwiched with ample epoxy resin between two brass plates. During extension in the tensile tester, the samples ruptured randomly. The highly drawn

Table I
Molecular Weights Evaluated by GPC and by Solution Viscosity for a SGC Mat of UHME-PE and for the Resultant Superdrawn Film[a]

	viscosity		GPC		
	$[\eta]$	10^4M_v	10^4M_n	10^4M_w	10^4M_z
SGC mat	15.3	188	18	140	410
drawn film (DR_t = 250)	15.3	188	20	150	430

[a] The GPC calibration with standard polystyrene is the likely origin of $M_v > M_w$.

films exhibited extensive fibrillation on tensile fracture.

The tensile strength, like modulus, increased rapidly at the lower DR_t and approached a constant value of 4.0 GPa at $DR_t > 200$. Films drawn to $DR_t > \sim 300$ often exhibited a lower strength, due to the formation of flaws revealed by the band structures in optical microscopy. The sample density also decreased at such high DR_t, as discussed later. The theoretical maximum tensile strength of polyethylene has been estimated to be 3.6[1] and 19 GPa,[35] by assuming the chain slippage and the chain rupture, respectively, for the mechanism of tensile fracture. Pennings et al.[36] found that the tensile strength of fully drawn polyethylene fibers increases with decreasing the fiber diameter. They estimate, based on a Griffice-type of relationship between the fiber diameter and the strength, that the theoretical maximum tensile strength is 26 GPa. The maximum strength of our films was 4.0 GPa, significantly lower than theory. The ultimate strength has been predicted to depend on the sample MW.[27,37] With sample MW a factor in determining the tensile properties, the extent of chain degradation during superdrawing of UHMW-PE SGC mats has been examined. Tests were made by solution viscosity and GPC. Table I shows this characterization of SGC mats and superdrawn films of DR_t 250. Within a fairly large experimental error, the GPC and intrinsic viscosity data show that no significant chain rupture occurred during superdrawing of SGC mats. It has been reported[38] that a significant chain rupture occurred on tensile drawing of melt-crystallized semicrystalline polymers, depending on the drawing conditions. The fact that no significant chain rupture occurs for superdrawing of UHMW-PE SGC mats is primarily ascribed to the lower draw stress and the absence of the strain hardening during draw (Figures 1, 7, and 8). Such deformation behavior is related to the specific morphology of the crystals isothermally precipitated from dilute solutions, i.e., the small number of entanglements and the well-developed lamellar crystals.

Effect of Drawing Technique. A significant influence of the technique for drawing SGC mats of UHMW-PE has been observed. The drawability, the efficiency of draw, as evaluated by tensile modulus versus DR, and hence the maximum achievable tensile properties. Among the techniques used, two-stage drawing, i.e., solid-state coextrusion of a mat to a low EDR of ~6 followed by tensile drawing at elevated temperatures, gave the most efficient and high draw, and hence the highest tensile properties, as cited above. Another remarkable effect of the drawing technique is found in the mode of unit cell orientation. Figure 14 shows sets of WAXD and SAXS patterns obtained with the incident beam parallel (left; A, C, and E) and perpendicular (right; B, D, and F) to the wide surface of the initial mat (A and B) for a DR 25 film tensile drawn (C and D) and an EDR 25 sample prepared by solid-state coextrusion both at 120 °C (E and F). The DR 25 corresponds to the natural draw for a SGC mat, where the neck propagated throughout the mat. The WAXD patterns of

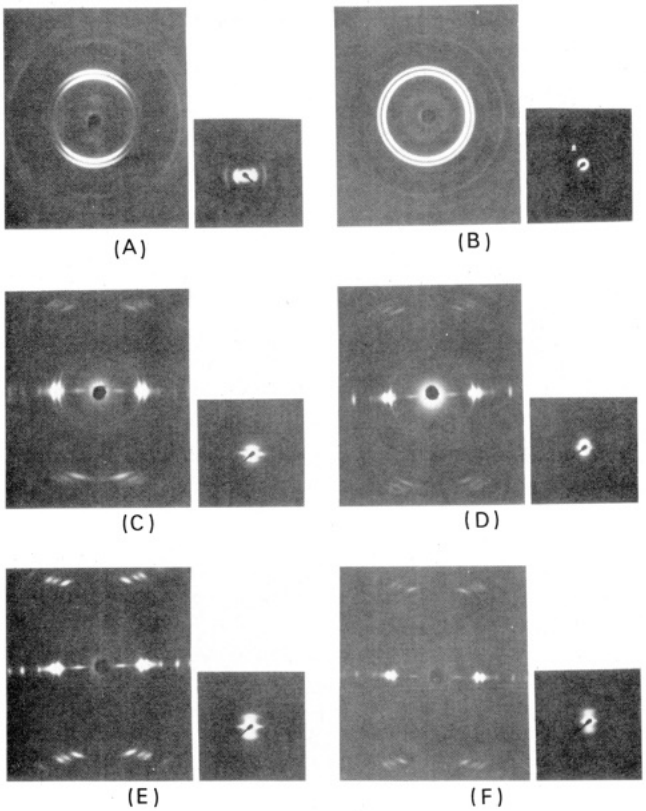

Figure 14. WAXD (left) and SAXS (right) patterns of an as formed mat (A and B), a DR 25 film prepared by tensile drawing of a mat at 120 °C (C and D), and an EDR 25 film drawn by solid-state coextrusion at 120 °C (E and F). The patterns were recorded with the incident beam parallel (left row) and perpendicular (right row) to the wide surface of the films.

all drawn samples show a weak reflection from the monoclinic cell, just inside the strong (110) orthorhombic reflections. The crystalline chain orientation at low DR was generally higher for solid-state coextrusion (parts E and F of Figure 14) than for tensile drawing (parts C and D of Figure 14). Further, when the incident beam was directed parallel to the surface of a tensile drawn film (Figure 14C), the (200) reflection became stronger than the (110) reflection and the (020) almost merged into the background. In contrast, when the beam was oriented perpendicular to the film surface (Figure 14D), the (110) reflection was strongest and the (020) became markedly stronger. These features indicate that the unit-cell *a* axis preferentially orients perpendicular to the film surface and the *b* axis parallel to the film surface, with both axes perpendicular to the fiber axis. The SAXS patterns of the tensile drawn film also revealed an anisotropic structure. The pattern obtained with the X-ray parallel to the film surface (Figure 14C) shows a meridional long period scattering much elongated perpendicular to the fiber axis compared to that for the beam perpendicular to the surface (Figure 14D). These SAXS features show that the lateral dimension of the microfibrils is significantly smaller in the film thickness (unit cell *a* axis) than through the film width (*b* axis) in tensile drawn films. In contrast, the WAXD and SAXS patterns of solid-state extrudate show a typical uniaxial fiber symmetry, independent of the incident X-ray beam direction (Figure 5 and parts E and F of Figure 14).

During tensile drawing of a mat, the thickness reduced markedly and the width only slightly, whereas on solid-state coextrusion each of the dimensions decreased by the same extent. This difference in macroscopic deformation likely explains the resultant difference in the unit-cell

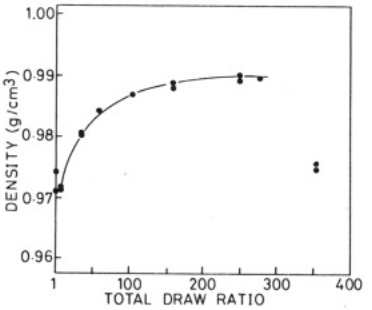

Figure 15. Density as a function of DR_t for doubly drawn films prepared from SGC mats of UHMW-PE.

orientation and the shape of microfibrils within the drawn samples. The selective reduction in the thickness on tensile drawing of the SGC mat indicates that crystal slippage proceeds preferentially within the plane parallel to the mat surface. During tensile deformation, the lamellae, initially oriented nearly parallel to the mat surface, are rotated and inclined to the draw direction. When the (200) plane comes to the highest shear position (~45° to the draw axis), neck deformation occurs through the crystal slippage in the (200) plane along the chain axis. Such a mechanism for tensile deformation explains well the formation of the single crystal-like texture as well as the lateral shape of microfibrils within the sample. For solid-state coextrusion no anisotropy in the cross-section is introduced. A similar effect has been observed on drawing melt-crystallized films of nylon 6.[40]

Morphology of Superdrawn Films. Figure 15 shows sample density as a function of DR_t for doubly drawn films. The density initially increased rapidly with DR_t and then approached a constant value of 0.988–0.990 g/cm³ in the DR_t range of 150–270. At a DR_t of 300, the density dropped, indicating extensive void formation. Densities reported here by the floatation in a liquid correspond to a minimum value, as the strong equatorial SAXS shows that the highly drawn films are highly fibrillated. A simple crystal–amorphous two-phase model may not be applicable to these ultraoriented, highly crystalline samples. Nevertheless, the crystallinity computed from such a model provides a measure for the morphological perfection of high modulus polyethylenes. Assuming the normal densities for amorphous (ρ_a = 0.854 g/cm³) and crystal (ρ_c = 1.00 g/cm³), the crystallinity increased from 83 wt % for the initial mat to ~94 wt % at a DR_t of 250. However, Adams et al.[39] found that the ρ_a of HDPE increases on solid-state extrusion up to 0.889 g/cm³ at an EDR of 36. With use of this amorphous density and the corresponding drawn crystal density of ρ_c = 0.995 g/cm³, the crystallinity of the superdrawn film (DR_t 250) is ~96 wt %. Despite ambiguities, it may be noted that the heats of fusion measured by DSC are 64–67 cal/g, corresponding to 93–97 wt % crystallinity, in agreement with the estimates from density. The birefringence of the superdrawn film, observed under an optical microscope, survived up to ~180 °C, indicating a chain orientation still remaining above the DSC melting point of 146 °C (3 °C/min). This suggests that the crystallinity from the heat of fusion is a minimum.

Figure 16 shows WAXD and SAXS patterns of a superdrawn film of DR_t 250. The WAXD pattern was recorded with a single film. Independent of both initial EDR and orientation of the incident beam, highly drawn films prepared by two-stage drawing show an uniaxial and extremely high chain orientation as revealed by the circular spots. This indicates that the characteristic orientation of the *a* and *b* axes observed for tensile drawn films is primarily determined when the initial lamellae transform

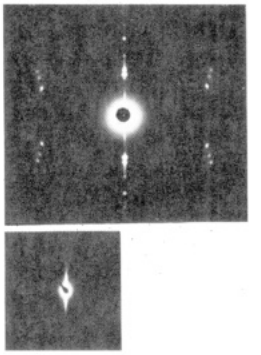

Figure 16. WAXD (left) and SAXS (right) patterns of a superdrawn UHMW-PE film with DR_t 250.

Table II
Structural Parameters of Superdrawn Ultrahigh Molecular Weight Polyethylene

	DR = 250	perfect crystal
ρ_{calcd} (g/cm³)	0.995	1.00
ρ_{obsd} (g/cm³)	0.986–0.990	
X_w (%)[a]	94–96	100
ΔH_f (cal/g)	64–67	69
X_w (%)[a]	93–97	100
D_{200} (Å)	190–260	
D_{110} (Å)	280–400	
D_{001} (Å)	710^G–$1490^{C\,c}$	
SAXS	no long period	
expansion coeff, $10^5\beta_{11}$ (1/°C)		
−60 to −30 °C	−1.16	−1.18[b]
30–60 °C	−1.46	−1.31[b]
f_c	~1	1

[a] Minimum estimate for the crystallinity. [b] Kobayashi, Y.; Keller, A. *Polymer* **1960**, *11*, 114. Davis, G. T. Eby, R. K.; Colson, J. P. *J. Appl. Phys.* **1970**, *41*, 4316. [c] G and C: Gaussian and Cauchy value, respectively.

to the fibrillar structure. Further deformation by tensile forces has no major effect on unit cell orientation. The WAXD pattern in Figure 16 shows a weak reflection from the monoclinic modification inside the orthorhombic (110) reflection. The appearance of the monoclinic cell was also confirmed by the pattern recorded with Cu Kα radiation monochromatized by a graphite monochrometer. The presence of such a metastable phase in superdrawn films, prepared even at 130 °C, suggests the existence of the local constraints in the samples.

The SAXS pattern in Figure 16 shows a very strong scattering on the equator and a less strong scattering around the direct beam. However, the long period scattering ascribed to the folded-chain crystals has disappeared. The intensity of this scattering generally decreases with increasing DR,[39,41] due to (1) the increase in the amorphous density, (2) the decrease in the crystal density, and (3) amount of chain folds. The quantitative evaluation of the changes in SAXS intensity has been reported by Adams et al.[39] for HDPE extrudates from EDR ⩽ 36. The extremely high chain orientation and the disappearance of the long period scattering, revealed by X-ray, indicate that most of the chain folds have been unravelled with the chains extended and oriented along the fiber axis after superdraw. Some additional structural parameters are also summarized in Table II.

Conclusions

Sedimented mats of UHMW-PE single crystals, grown from dilute solutions in xylene, have been uniaxially drawn by the three techniques of solid-state coextrusion, conventional tensile drawing, and the sequential combination

of the two (two-stage drawing). The mats exhibited a high extensibility and could be drawn to over a DR of 200 by these techniques under controlled conditions. However, the drawing behavior and the resultant structure and tensile properties are markedly affected by the technique. The coherency of the initial mats also had a major effect on the drawability and efficiency of tensile draw, whereas no such effects were present in solid-state coextrusion and for two-stage draw. Two-stage draw, i.e., solid-state coextrusion to a low EDR of ~6 followed by tensile drawing at elevated temperatures, gave the most efficient and high draw. The tensile modulus and strength of such doubly drawn films increase rapidly with DR in the low range ($DR_t < 150$) and approach a constant value of 210–220 and 4.0 GPa, respectively, at high a DR_t of $\geq$200–250, for a polyethylene MW of 1.6×10^6. Tensile drawing produces a single crystal-like texture, whereas the other two techniques produce a typical uniaxial orientation. WAXD, SAXS, density, heat of fusion, and linear expansivity reveal the extremely high chain extension, orientation and morphological perfection of the superdrawn, ultrahigh modulus and strength films of UHMWPE prepared from SGC mats.

Registry No. Polyethylene, 9002-88-4.

References and Notes

(1) Ciferri, A., Ward, I. M., Eds. *Ultra-High Modulus Polymers*; Applied Science: London, 1978.
(2) Zachariades, A. E., Porter, R. S., Eds. *Strength and Stiffness of Polymers*; Plastic Engineering Series, Marcel Dekker: New York, 1983; Vol. 4.
(3) Inoue, N., Ichihara, M., Eds. *Hydrostatic Extrusion; Theory and Applications*; Elsevier Applied Science: London, 1985.
(4) Lemstra, P. J.; Kirschbaum, R. *Polymer* **1985**, *26*, 1372.
(5) Southern, J. H.; Porter, R. S. *J. Macromol. Sci.* **1970**, *4*, 541.
(6) Zachariades, A. E.; Mead, W. T.; Porter, R. S. *Chem. Rev.* **1980**, *80*, 351.
(7) Imada, K.; Yamamoto, T.; Shigematsu, K.; Takayanagi, M. *J. Mater. Sci.* **1971**, *6*, 537.
(8) Capaccio, G.; Compton, T. A.; Ward, I. M. *J. Polym. Sci., Polym. Phys. Ed.* **1976**, *14*, 1641.
(9) Barham, P. J.; Keller, A. *J. Mater. Sci.* **1976**, *11*, 27.
(10) Perkins, W. G.; Capiati, N. J.; Porter, R. S. *Polym. Eng. Sci.* **1976**, *16*, 200.
(11) Zwijnemberg, A.; Pennings, A. J. *Colloid Polym. Sci.* **1976**, *254*, 868.
(12) Smith, P.; Lemstra, P. J.; Booij, H. C. *Colloid Polym. Sci.* **1980**, *258*, 891.
(13) Smith, P.; Lemstra, P. J.; Pijper, J. P. L.; Kiel, A. M. *Colloid Polym. Sci.* **1981**, *259*, 1070.
(14) Sakurada, I.; Ito, T.; Nakamae, K. *J. Polym. Sci., Part C* **1966**, *15*, 75.
(15) Obser, G.; Blasenberg, S. *Colloid Polym. Sci.* **1970**, *241*, 985.
(16) Matsuo, M.; Sawatari, C. *Macromolecules* **1986**, *19*, 2036.
(17) Mead, W. T.; Desper, C. R.; Porter, R. S. *J. Polym. Sci., Polym. Phys. Ed.* **1979**, *17*, 859.
(18) Kanamoto, T.; Sherman, E. S.; Porter, R. S. *Polymer J.* **1979**, *11*, 497.
(19) Statton, W. O. *J. Appl. Phys.* **1967**, *38*, 4149.
(20) Ishikawa, K.; Miyasaka, K.; Maeda, M. *J. Polym. Sci., Polym. Phys. Ed.* **1970**, *7*, 2029.
(21) Kanamoto, T.; Tsuruta, A.; Tanaka, K.; Takeda, M.; Porter, R. S. *Polym. J.* **1983**, *15*, 327.
(22) Kanamoto, T.; Tsuruta, A.; Tanaka, K.; Takeda, M.; Porter, R. S. *Rep. Prog. Polym. Phys. Jpn.* **1983**, *26*, 347.
(23) Griswold, P. D.; Zachariades, A. E.; Porter, R. S. *Polym. Eng. Sci.* **1978**, *18*, 861.
(24) Kanamoto, T.; Tsuruta, A.; Tanaka, K.; Takeda, M. *Polym. J.* **1984**, *16*, 75.
(25) Furuhata, K.; Yokokawa, T.; Miyasaka, K. *J. Polym. Sci., Polym. Phys. Ed.* **1984**, *22*, 133.
(26) Matsuo, M.; Sawatari, C.; Iida, M.; Yoneda, M. *Polym. J.* **1985**, *17*, 1179.
(27) Kanamoto, t.; Tanaka, K.; Takeda, M.; Porter, R. S. American Chemical Society Workshop, "Flow Deformation and Molecular Reorganization in Polymers with Crystalline and Liquid Crystalline Order", April 1986, Montreal, Canada.
(28) Geil, P. H., Ed. *Polymer Single Crystals*; Interscience: New York, 1963.
(29) Nakafuku, C.; Takemura, T. *Mem. Fac. Eng., Kyushu Univ.* **1974**, *34*, 11.
(30) Kanamoto, T.; Porter, R. S. *Polym. Prepr., Jpn*, **1983**, *32* (4), 744.
(31) Kanamoto, T.; Ohama, T.; Tanaka, K.; Takeda, M.; Porter, R. S., submitted for publication in *Polym. Commun.*
(32) Kanamoto, T.; Ito, M.; Ogura, K.; Tanaka, K.; Porter, R. S. *Polymers for Fibers and Elastomers*; ACS Symposium Series 260; Arthur, J. C., Jr., Ed., American Chemical Society: Washington, DC, 1984.
(33) Takayanagi, M.; Kajiyama, T. *J. Macromol. Sci., Phys., B-8* **1973**, 1.
(34) Ito, M.; Tanaka, K. *Rep. Prog. Polym. Phys. Jpn.* **1986**, *24*, 273.
(35) Boudreaux, D. P. *J. Polym. Sci., Polym. Phys. Ed.* **1973**, *11*, 1285.
(36) Pennings, A. J.; Smook, J.; Boer, J.; Goglewski, S.; Hutten, P. F. *Pure Appl. Chem.* **1983**, *55*, 777.
(37) Termonia, Y.; Meakin, P.; Smith, P. *Macromolecules* **1985**, *18*, 2246.
(38) Stoeckel, T. M.; Blasius, J.; Crist, B. *J. Polym. Sci., Polym. Phys. Ed.* **1978**, *16*, 485.
(39) Adams, W. W.; Briber, R. M.; Sherman, E. S.; Porter, R. S.; Thomas, E. L. *Polymer* **1985**, *26*, 17.
(40) Kanamoto, T.; Zachariades, A. E.; Porter, R. S. *J. Polym. Sci., Polym. Phys. Ed.* **1982**, *20*, 1485.
(41) Peterlin, A.; Corneliussen, R. *J. Polym. Sci., Polym. Phys. Ed.* **1968**, *6*, 1273.